Determination of Monochloramine Formation Rate Constants with Stopped-Flow Spectrophotometry

ARTICLE *in* ENVIRONMENTAL SCIENCE AND TECHNOLOGY · MARCH 2004

Impact Factor: 5.33 · DOI: 10.1021/es0347484 · Source: PubMed

2 AUTHORS:

Zhimin Qiang
Chinese Academy of Sciences
92 PUBLICATIONS **1,863** CITATIONS
SEE PROFILE

Craig Adams
Utah State University
92 PUBLICATIONS **2,623** CITATIONS
SEE PROFILE

Environ. Sci. Technol. **2004**, *38,* 1435−1444

Determination of Monochloramine Formation Rate Constants with Stopped-Flow Spectrophotometry

ZHIMIN QIANG AND CRAIG D. ADAMS*

Environmental Research Center, Department of Civil, Architectural and Environmental Engineering, University of Missouri−Rolla, Rolla, Missouri 65409

The production of monochloramine by the reaction of aqueous ammonia and free chlorine is important in both drinking water and wastewater treatment systems. Accurate prediction of the rate of monochloramine formation is a prerequisite for any modeling work related to this fundamental reaction. There are significant discrepancies between rate constants reported in the literature. Furthermore, little information is available on the temperature dependence of the reaction rate constant. The purposes of this study were to kinetically examine the potential reaction pathways, accurately determine the specific rate constants, and establish the Arrhenius equation for the reaction of monochloramine formation using the stopped-flow technique. Results indicate that the rate constants are highly pH dependent due to the speciation of both free chlorine and ammonia. From a strictly kinetic point of view, monochloramine formation could be explained by either the nonionic pathway between HOCl and NH_3 or the ionic pathway between OCl^- and NH_4^+. However, because the ionic pathway is mechanistically implausible the reaction is shown to be between the nonionic species (HOCl and NH_3). The specific rate constant for the nonionic pathway at 25 °C was determined to be 3.07×10^6 ($M^{-1}\cdot s^{-1}$). The Arrhenius equation was obtained as $k_{HOCl,NH_3} = 5.40 \times 10^9 \exp(-2237/T)$, which provided an activation energy of 18.6 $kJ\cdot mol^{-1}$.

Introduction

Free chlorine is used extensively in the United States to disinfect drinking, waste, and cooling waters (*1, 2*). If ammonia is present in water, chloramines are formed which can be utilized as secondary disinfectants. The simplified chlorine−ammonia reactions are described as follows (*3*):

$$HOCl + NH_3 \rightarrow NH_2Cl + H_2O \quad \text{(monochloramine)} \quad (1)$$

$$HOCl + NH_2Cl \rightarrow NHCl_2 + H_2O \quad \text{(dichloramine)} \quad (2)$$

$$HOCl + NHCl_2 \rightarrow NCl_3 + H_2O \quad \text{(trichloramine)} \quad (3)$$

These competitive reactions are primarily dependent on pH and the chlorine:ammonia-nitrogen (Cl_2:N) ratio. In the pH range of 6.5−8.5, monochloramine (MCA) is predominantly formed at Cl_2:N ratios ≤ 5:1 by weight. At Cl_2:N ratios ≥ 7.6:1, breakpoint chlorination occurs, leading to the formation of nitrogen gas, nitrate, nitrogen chloride, and the recurrence of free chlorine. For chloramination, utilities generally apply a Cl_2:N weight ratio between 3 and 5 (*4*). This ratio is generally used to balance the risk of trihalomethanes (THM)/haloacetic acids (HAA) formation with the risk of distribution system nitrification. MCA also provides better protection against bacterial regrowth in water distribution and wastewater treatment systems. The stringent regulations regarding disinfection byproducts (DBPs) generation and bacterial regrowth have increased the popularity of chloramination (*5*). Many synthetic organic chemicals (SOCs) may react rapidly with free chlorine, yet only slowly with MCA. Thus, when free chlorine and ammonia are added to a solution containing reactive SOCs, the relative rate of reaction of free chlorine with ammonia versus free chlorine with SOCs is of critical importance. Therefore, the kinetics of MCA formation is a key concern for both water and wastewater treatment.

The kinetics of MCA formation has been extensively investigated by numerous researchers (*6*−*11*). However, the previous studies were hindered by either the rapid reaction kinetics or the interference from side reactions, resulting in significant discrepancies between the rate constants reported in the literature. In a critical review paper, Morris and Isaac (*12*) collected the available experimental data of MCA formation rates at various temperatures and pH values from several researchers (*6*, *10*−*11*) and based on these data sources approximated an Arrhenius equation of $k = 6.6 \times 10^8 \exp(-1510/T)$. It is noted, however, that the reaction rates from different researchers are considerably scattered. For example, the rate of MCA formation varied from 1.9×10^6 to 6.2×10^6 $M^{-1}\cdot s^{-1}$ at 25 °C, a 3-fold difference (*12*). If only the experimental data from Weil and Morris (*6*) were plotted, the resultant Arrhenius equation was $k = 2.5 \times 10^{10} \exp(-1259/T)$. The reaction of MCA formation proceeds so rapid that the rate is only measurable by ordinary techniques at very low reactant concentrations on the order of magnitude of 10^{-5} M either below pH 6.5 or above pH 11 (*6*, *7*, *13*). The low reactant concentrations, the limited pH range and the calculation of rate constants merely based on the initial period of reaction may easily lead to significant analysis errors in the determination of MCA formation rates. Another major point is that some researchers (*6*, *8*) worked at high Cl_2:N ratios, which potentially promotes side reactions such as dichloramine or even trichloramine formation.

Due to the critical importance of accurate knowledge concerning the reaction rate between free chlorine and ammonia in drinking water and wastewater systems, there is a significant need to revise the rate constants of MCA formation over a range of pH values and temperatures typical for water and wastewater treatment when modern analytical techniques become available. In this work, we directly measured the rate constants of MCA formation using the stopped-flow technique over the pH range of 6−12 and temperature range of 5−35 °C. In addition, all four potential reaction pathways based on speciation of free chlorine and ammonia were examined by model computations, and the reaction mechanism was proposed from our kinetic data in combination with the mechanistic information obtained from literature. The objectives of this study were to kinetically examine the potential pathways, determine the specific rate constants, and establish the Arrhenius equation for the reaction of MCA formation with a significantly improved accuracy.

* Corresponding author phone: (573)341-4041; fax: (573)341-7217; e-mail: adams@umr.edu. Mailing address: 220 Butler-Carlton Hall, Department of Civil, Architectural and Environmental Engineering, University of Missouri−Rolla, Rolla, MO 65409.

10.1021/es0347484 CCC: $27.50
Published on Web 01/28/2004

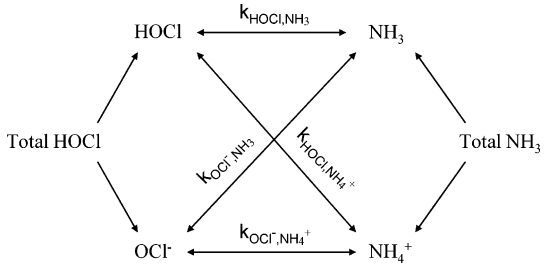

FIGURE 1. Schematic diagram of potential reaction pathways of MCA formation.

Model Description

The overall reaction of MCA formation is described by reaction 1 where HOCl and NH_3 represent the total free chlorine and ammonia present in aqueous solution, respectively. The rate of MCA formation is expressed by the following second-order equation

$$\frac{d[MCA]}{dt} = -\frac{d[HOCl]_T}{dt} = k_{obs}''[HOCl]_T[NH_3]_T \quad (4)$$

where k_{obs}'' = derived second-order rate constant, $[HOCl]_T$ = total concentration of free chlorine ($HOCl + OCl^-$), $[NH_3]_T$ = total concentration of ammonia ($NH_4^+ + NH_3$). If ammonia is applied in 10-fold excess with respect to free chlorine, $[NH_3]_T$ can be viewed as approximately constant. Thus, eq 4 is simplified to a pseudo-first-order equation

$$\frac{d[MCA]}{dt} = k_{obs}'[HOCl]_T \quad (5)$$

where

$$k_{obs}' = k_{obs}''[NH_3]_T \quad (6)$$

The pseudo-first-order rate constant, k_{obs}', can be directly determined by model fitting of experimental kinetic data.

In aqueous solutions, the speciation of free chlorine and ammonia is controlled by their ionization constants and solution pH

$$HOCl \leftrightarrow H^+ + OCl^-, K_{a,Cl} = \frac{\{H^+\}\{OCl^-\}}{\{HOCl\}} = \frac{[H^+][OCl^-]}{[HOCl]} \cdot \frac{\gamma_{H^+}\gamma_{OCl^-}}{\gamma_{HOCl}} \quad (7)$$

$$NH_4^+ \leftrightarrow H^+ + NH_3, K_{a,N} = \frac{\{H^+\}\{NH_3\}}{\{NH_4^+\}} = \frac{[H^+][NH_3]}{[NH_4^+]} \cdot \frac{\gamma_{H^+}\gamma_{NH_3}}{\gamma_{NH_4^+}} \quad (8)$$

where $K_{a,Cl}$ and $K_{a,N}$ are the ionization constants of HOCl and NH_4^+, respectively, and γ_{H^+}, γ_{OCl^-}, γ_{HOCl}, γ_{NH_3}, and $\gamma_{NH_4^+}$ represent the activity coefficients of reacting species. At 25 °C, $pK_{a,Cl}$ equals 7.537 (*14*) and $pK_{a,N}$ equals 9.251 (*15*). Based on the reactants speciation (charged or neutral), the overall reaction is considered to consist of four potential reaction pathways, as illustrated in Figure 1. These reactions are written as follows

$$HOCl + NH_3 \xrightarrow{k_{HOCl,NH_3}} NH_2Cl + H_2O \quad (9)$$

$$HOCl + NH_4^+ \xrightarrow{k_{HOCl,NH_4^+}} NH_2Cl + H_2O + H^+ \quad (10)$$

$$OCl^- + NH_3 \xrightarrow{k_{OCl^-,NH_3}} NH_2Cl + OH^- \quad (11)$$

$$OCl^- + NH_4^+ \xrightarrow{k_{OCl^-,NH_4^+}} NH_2Cl + H_2O \quad (12)$$

where k_{HOCl,NH_3}, k_{HOCl,NH_4^+}, k_{OCl^-,NH_3}, and k_{OCl^-,NH_4^+} represent the specific second-order rate constants for corresponding reaction pathways. Reaction 9 occurs by a nonionic mechanism between two neutral molecules, reactions 10 and 11 by a hybrid mechanism between an ion and a neutral molecule, and reaction 12 by an ionic mechanism between a cation and an anion. In the case of reaction 9, the rate of MCA formation is expressed by

$$\frac{d[MCA]}{dt} = k_{HOCl,NH_3}[HOCl][NH_3] \cdot \frac{\gamma_{HOCl}\gamma_{NH_3}}{\gamma_x} \quad (13)$$

where γ_x is the activity coefficient of activated complex (an unstable combination of reacting species that is intermediate between reactants and products) (*16*). At a given pH, the concentrations of un-ionized HOCl and NH_3 can be expressed in terms of their total concentrations through pK_a and proton activity:

$$[HOCl] = \frac{[HOCl]_T}{1 + \frac{K_{a,Cl}}{[H^+]} \cdot \frac{\gamma_{HOCl}}{\gamma_{H^+}\gamma_{OCl^-}}} \quad (14)$$

$$[NH_3] = \frac{[NH_3]_T}{1 + \frac{[H^+]}{K_{a,N}} \cdot \frac{\gamma_{H^+}\gamma_{NH_3}}{\gamma_{NH_4^+}}} \quad (15)$$

Substituting eqs 14 and 15 into eq 13 gives

$$\frac{d[MCA]}{dt} = \frac{k_{HOCl,NH_3}[HOCl]_T[NH_3]_T}{\left(1 + \frac{K_{a,Cl}}{[H^+]}\frac{\gamma_{HOCl}}{\gamma_{H^+}\gamma_{OCl^-}}\right)\left(1 + \frac{[H^+]}{K_{a,N}}\frac{\gamma_{H^+}\gamma_{NH_3}}{\gamma_{NH_4^+}}\right)} \cdot \frac{\gamma_{HOCl}\gamma_{NH_3}}{\gamma_x} \quad (16)$$

In a dilute solution, the activity coefficients of neutral molecules are taken as unity ($\gamma_{HOCl} = \gamma_{NH_3} = 1$), while the activity coefficients of all the monovalent ions are equal ($\gamma_{H^+} = \gamma_{OCl^-} = \gamma_{NH_4^+} = \gamma$). The value of γ_x is pertinent to the charge of the activated complex, i.e., $\gamma_x = 1$ for reactions 9 and 12 where the activated complex is supposed to be neutral, and $\gamma_x = \gamma$ for reactions 10 and 11 where the activated complex is supposed to be monovalent. Proton activity is directly measurable with a pH meter which is calibrated with NBS standard buffers, i.e., $\{H^+\} = 10^{-pH}$. Thus, the proton activity is directly used in our models instead of proton concentration. Moreover, the influence of liquid junction potentials can be ignored when the ionic strength of a solution is less than 0.1 M (*16*). Thus, eq 16 can be simplified to

$$\frac{d[MCA]}{dt} = k_{HOCl,NH_3}\frac{\gamma\{H^+\}}{\gamma\{H^+\} + K_{a,Cl}} \cdot \frac{\gamma K_{a,N}}{\gamma K_{a,N} + \{H^+\}}[HOCl]_T[NH_3]_T \quad (17)$$

If we assume that reaction 9 is the predominant pathway, eq

17 is approximately equal to eq 4. Thus, k_{obs}'' can be expressed in terms of k_{HOCl,NH_3}:

$$k_{obs}'' = k_{HOCl,NH_3}\frac{\gamma\{H^+\}}{\gamma\{H^+\} + K_{a,Cl}} \cdot \frac{\gamma K_{a,N}}{\gamma K_{a,N} + \{H^+\}} \quad (18)$$

The plot of k_{obs}'' vs $(\gamma\{H^+\}/(\gamma\{H^+\} + K_{a,Cl}))\cdot(\gamma K_{a,N}/(\gamma K_{a,N} + \{H^+\}))$ will yield a straight line with its slope equaling k_{HOCl,NH_3} and its intercept equaling zero if the assumption is valid. In analogy, the k_{obs}'' can also be expressed in terms of k_{HOCl,NH_4^+}, k_{OCl^-,NH_3}, and k_{OCl^-,NH_4^+} according to reactions 10−12, respectively:

$$k_{obs}'' = k_{HOCl,NH_4^+}\frac{\gamma\{H^+\}}{\gamma\{H^+\} + K_{a,Cl}} \cdot \frac{\{H^+\}}{\gamma K_{a,N} + \{H^+\}} \quad (19)$$

$$k_{obs}'' = k_{OCl^-,NH_3}\frac{K_{a,Cl}}{\gamma\{H^+\} + K_{a,Cl}} \cdot \frac{\gamma K_{a,N}}{\gamma K_{a,N} + \{H^+\}} \quad (20)$$

$$k_{obs}'' = k_{OCl^-,NH_4^+}\gamma^2\frac{K_{a,Cl}}{\gamma\{H^+\} + K_{a,Cl}} \cdot \frac{\{H^+\}}{\gamma K_{a,N} + \{H^+\}} \quad (21)$$

The value of γ can be calculated by the Güntelberg approximation which is suitable for a solution containing several electrolytes with an ionic strength less than 0.1 M (*16*)

$$\log\gamma = -Az^2\frac{\sqrt{I}}{(1+\sqrt{I})} \quad (22)$$

where $A \approx 0.5$ for a water solution, z = charge of ion, and I (ionic strength) $= 0.5\sum C_i z_i^2$. In this study, the ionic strength of reaction solutions was controlled by 50 mM $NaClO_4$. The total ionic strength was approximately equal to 0.075 M if the reactants, buffer, and acid or base added for pH adjustment were all counted. Thus, γ was calculated to be 0.78.

In brief, our modeling scheme is described as follows: first determine k_{obs}' by model fitting the kinetic traces obtained by the stopped-flow using a pseudo-first-order equation; then calculate k_{obs}'' by dividing k_{obs}' by the initial concentration of ammonia; and finally plot k_{obs}'' vs the activity products of reacting species to determine the specific rate constants of potential reaction pathways.

Experimental Section

Reagents. All chemicals were used as received. Ammonium chloride (certified ACS, 99.5%), potassium phosphate monobasic (HPLC grade, 99.6%), sodium borate (certified ACS, 101.1%), sodium perchlorate (HPLC grade), perchloric acid (trace metal grade, 67−71%), and sodium hydroxide (certified ACS, 98.7%) were purchased from Fisher Scientific (Pittsburgh, PA). Sodium hypochlorite solution (minimum 4%) from Aldrich (Milwaukee, WI) was used as the source of free chlorine. Millipore water was produced by a water purification system (Model Simplicity 185, Millipore Co., Bedford, MA) after distillation and deionization, with a final resistivity of ≥ 18.2 MΩ·cm. This Millipore water was used to prepare all reaction solutions in this study. Working solutions of ammonium chloride and sodium hypochlorite were freshly prepared every day and stored in amber bottles to prevent possible degradation by lights. KH_2PO_4 and $Na_2B_4O_7$ were used as buffers for the pH ranges of 6−9.5 and 10−12, respectively. NaOH and $HClO_4$ solutions prepared at a series of appropriate concentrations were used for pH adjustment. The ionic strength of reaction solutions was controlled with 50 mM $NaClO_4$.

Analysis. The concentration of sodium hypochlorite stock solution was experimentally determined to be 4.8% by the DPD Total Chlorine AccuVac Ampul Method (HACH Co., Loveland, CO). Working solutions of sodium hypochlorite were prepared by diluting this stock solution. A digital pH meter (Model 320) coupled with a combination pH probe, both from Corning Inc. (Corning, NY), was used to measure solution pH. This pH meter was calibrated with NBS standard buffers purchased from Fisher Scientific (Pittsburgh, PA), i.e., pH 4.00 ± 0.01, 7.00 ± 0.01, and 10.00 ± 0.02.

Procedures. To determine the UV-absorption spectra of HOCl/OCl^- and MCA as a function of pH, MCA was prepared by mixing the solutions of HOCl and NH_4Cl with 10% excess ammonia. The yield was determined to be 98% of theoretical production. Both HOCl/OCl^- and MCA solutions were adjusted to an initial pH 10 immediately after preparation. The pH was first titrated downward by dropwise addition of $HClO_4$ solution and then titrated upward by dropwise addition of NaOH solution. At preselected pH values, the ultraviolet absorption spectra were measured with a conventional spectrophotometer (Model Cary 50 Conc., Varian Australia PTY LTD, Australia).

To determine the rate constants of MCA formation, a stopped-flow spectrophotometer (Model SX.18MV-R, Applied Photophysics Co., Leatherhead, UK) was used to conduct kinetic experiments. This stopped-flow had one reaction cell of 20 μL with a dead time (or mixing time) of about 1.5 ms and was able to determine a first-order rate constant up to 3000 s^{-1}. A 150W xenon lamp was used as the light source, and an emission photomultiplier was used as the detector. Temperature was controlled by an automatic water circulator (Model 3016, Fisher Scientific, Pittsburgh, PA) connected to the sample handling unit of the stopped-flow. Control of the stopped-flow and acquisition of kinetic data were carried out by a RISC computer workstation. Kinetic data were analyzed by the Pro/K software (Applied Photophysics).

In the kinetic experiments, NH_4Cl (10 mM) and HOCl (1 mM) solutions were employed with a molar ratio of 10:1. In the presence of excess ammonia, the hydrolysis of MCA and its decomposition to dichloramine and trichloramine were both depressed (*12*). The reactants solutions were preadjusted to the same initial pH and buffered with 10 mM phosphate or borate, and ionic strength was controlled with 50 mM $NaClO_4$. An equal volume (50 μL) of NH_4Cl and HOCl solutions were simultaneously injected into the photocell of the stopped-flow with two automatic nitrogen-driven syringes. In parallel, 10 mL of each reactant solution was mixed in a beaker under the same experimental conditions to measure the final reaction pH. The reaction pH ranged from 6 to 12, and temperatures were controlled at 5, 15, 25, and 35 °C. At each preselected pH, five replicate kinetic traces were obtained using the stopped-flow with at least 90% completion of the reaction. The pseudo-first-order rate constant at a given pH was calculated by averaging five individual rates with the standard error reported. Then, the second-order rate constant was derived by dividing the pseudo-first-order rate constant by the initial concentration of ammonia. Both OCl^- decay and MCA production were monitored at wavelengths of 294 and 243 nm, respectively. In addition, the rapid scanning mode of the stopped-flow was utilized to monitor the absorbance over a wavelength range of 225−315 nm (10 nm interval).

Our preliminary experiments show that all the solutions of ammonium chloride, sodium phosphate monobasic, sodium borate, sodium hydroxide, and perchloric acid were transparent to light absorbance at the detection wavelengths for OCl^- and MCA. This result was desirable for the stopped-flow because there was no spectral interference with the absorbance measurement of OCl^- and MCA from these chemical species.

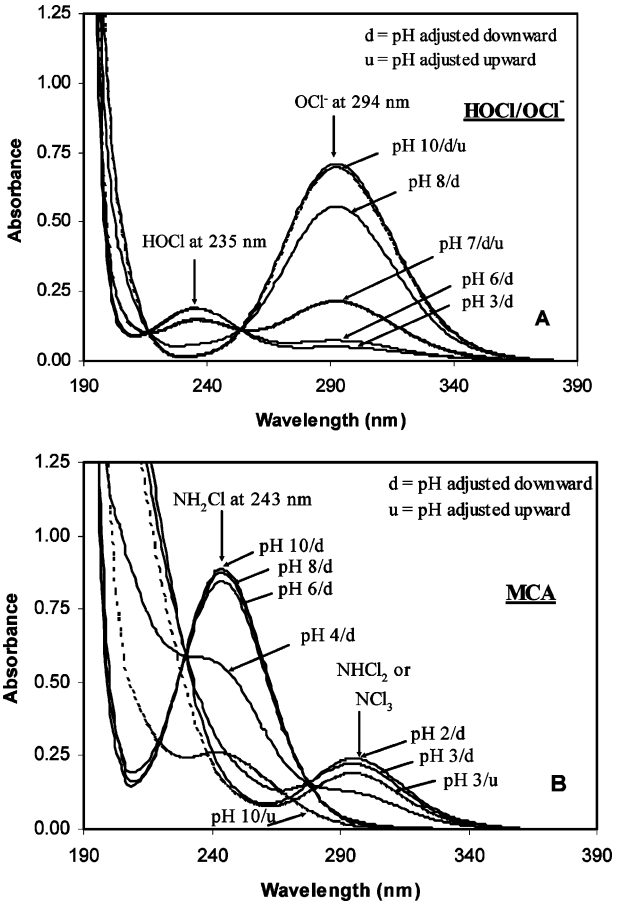

FIGURE 2. UV spectra as a function of pH: (A) 2 mM HOCl and (B) 2 mM MCA.

Results and Discussion

UV-Absorption Spectra of HOCl/OCl⁻ and MCA. The stopped-flow measures the UV−VIS absorbance change of either reactant decay or product formation to determine the reaction rate constant. The spectra of reactants and products would be analytically informative on the selection of appropriate monitoring wavelength for the stopped-flow.

The UV spectra of HOCl/OCl⁻ (2 mM) from pH 3 to 10 are shown in Figure 2A. The pK_a of HOCl controls the emergence of absorption peaks at a given pH. Results indicate that the maximum molar absorptivity is 355 $M^{-1}\cdot cm^{-1}$ at 294 nm for OCl⁻ and 95 $M^{-1}\cdot cm^{-1}$ at 235 nm for HOCl. These results are comparable with 348 $M^{-1}\cdot cm^{-1}$ at 294 nm for OCl⁻ and 120 $M^{-1}\cdot cm^{-1}$ at 228 nm for HOCl (*17*), 350 $M^{-1}\cdot cm^{-1}$ at 292 nm for OCl⁻, and 100 $M^{-1}\cdot cm^{-1}$ at 235 nm for HOCl (*14*). At pH 7 and 10, the spectra of the downward and upward titrations are almost identical. It implies that the protonation of OCl⁻ and deprotonation of HOCl are totally reversible, i.e., no active chlorine loss during pH adjustment.

The spectra of MCA (2 mM) from pH 2 to 10 are shown in Figure 2B. Gray et al. (*18*) reported that $K_{NH_3Cl^+}$ was equal to 28 M^{-1} at 25 °C and ionic strength of 0.5 M (i.e., $pK_a = -1.45$). It is seen that MCA will neither protonate nor deprotonate significantly in the pH range of this work. Experimental results indicate that the maximum molar absorptivity of MCA is 445 $M^{-1}\cdot cm^{-1}$ at 243 nm, agreeing with the values reported previously (*8, 17, 19*). From pH 10 to 6, similar spectra are observed with only one peak at 243 nm which denotes MCA. The maximum absorbance at 243 nm decreases slightly with decreased pH probably due to enhanced MCA decay at lower pH values. At pH 4 and below, a new peak emerges at 294 nm. When the MCA solution is titrated backward to pH 10, the 294 nm peak disappears, but

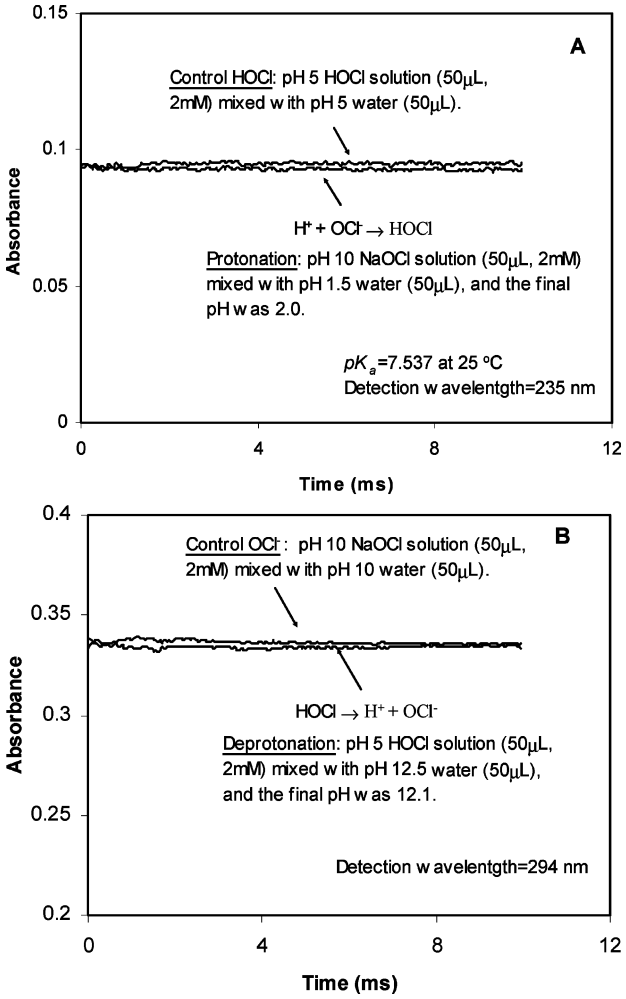

FIGURE 3. Instantaneous protonation and deprotonation: (A) protonation of OCl⁻ and (B) deprotonation of HOCl.

the recurred 243 nm peak only shows an absorbance of 0.26 AU. Compared with the original absorbance of 0.89 AU at pH 10, about 70% of MCA is gone. It is evident that MCA is not reversible during pH adjustment due to the occurrence of side reactions.

When MCA solution was acidified to pH 3.5−4.0, dichloramine ($NHCl_2$) was formed:

$$2NH_2Cl + H^+ \leftrightarrow NHCl_2 + NH_4^+ \qquad (23)$$

If the pH was further decreased, trichloramine (NCl_3) would be produced. The molar absorptivities of $NHCl_2$ and NCl_3 were determined to be 276 and 160 $M^{-1}\cdot cm^{-1}$, respectively, both at 294 nm as a local absorption maximum (*20*). Neither $NHCl_2$ nor NCl_3 is stable, and their decomposition to N_2, Cl^-, and other possible products results in the loss of oxidizing materials (i.e., chloramines). We should point out that there are two clearly different mechanisms accounting for the MCA loss in chlorine−ammonia systems though both are initiated by OH^- catalysis involving dichloramine. One is predominant in the presence of excess ammonia when free chlorine concentration is extremely low (*21*), and the other is predominant in the presence of measurable amounts of free chlorine (*20*). In our UV spectra experiments, MCA was formed with 10% excess ammonia. Thus, the observed permanent loss of MCA when adjusting pH back to 10 should follow the HOCl independent mechanism proposed by Jafvert and Valentine (*21*) more closely.

To avoid the interference from MCA decomposition at low pH values, the stopped-flow kinetic experiments of MCA

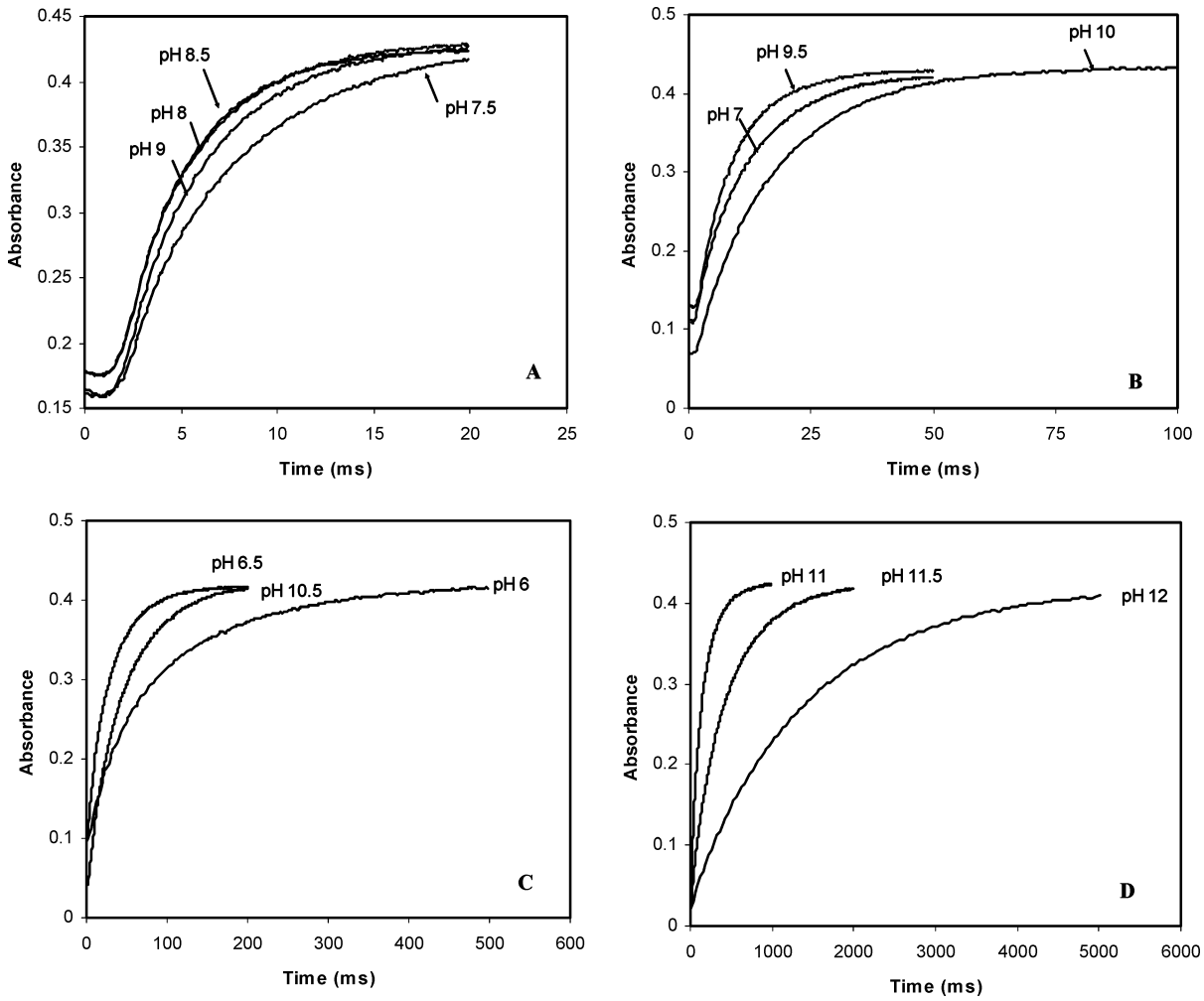

FIGURE 4. Kinetic traces of MCA formation as a function of initial pH: (A) pH 7.5−9; (B) pH 7, 9.5 and 10; (C) pH 6, 6.5, and 10.5; (D) pH 11−12. Experimental conditions: 10 mM NH_4Cl, 1 mM HOCl, 50 mM $NaClO_4$, 10 mM buffer (phosphate for pH 6−9.5, borate for pH 10−12), 25 °C.

formation were conducted at pH 6 and above in the presence of excess ammonia. It should be noted that the HOCl independent mechanism of dichloramine decomposition was suspected but not important under our experimental conditions because MCA formation (0.02−5 s, this study) was much faster than dichloramine decomposition (about 25 min) (*21*). The UV-absorption spectra in Figure 2A,B show that the rate of MCA formation may be determined by monitoring either OCl^- decay at 294 nm or MCA production at 243 nm. However, there is usually a small change between the original and final pH values. As a result, the change in OCl^- absorbance (294 nm) is partially caused by the protonation of OCl^- or deprotonation of HOCl, not totally reflecting the rate of MCA formation. Therefore, the reaction rate was primarily measured by monitoring MCA production at 243 nm, while OCl^- decay at 294 nm was monitored as a reference.

Instantaneous Protonation/Deprotonation. Our mathematical models for rate constant computation are based on the speciation of free chlorine and ammonia. These models have a fundamental assumption: the protonation and deprotonation of reacting species are instantaneous (<1.5 ms), hence, are not rate-limiting. To be "instantaneous", the protonation and deprotonation reactions should proceed much faster than MCA formation.

The rates of protonation of OCl^- and deprotonation of HOCl were qualitatively examined using the stopped-flow. Two nearly flat absorbance curves are shown in Figure 3A: one for OCl^- protonation, and the other for a control. Our results indicate that the protonation of OCl^- proceeds too fast to be observable via the stopped-flow (i.e., <1.5 ms).

Similar results were obtained for the deprotonation of HOCl, as shown in Figure 3B. Therefore, the assumption of instantaneous protonation and deprotonation relative to the kinetics of MCA formation is validated.

pH Dependence of MCA Formation Rate. The kinetic traces of the reaction of MCA formation from pH 6 to 12 are shown in Figure 4. Results indicate that the reaction rate is strongly pH dependent. MCA is produced most rapidly in the pH range of 7.5−9 with the reaction being completed in 20 ms (Figure 4A). The complete reaction requires approximately 50−500 ms in pH 6−7 and 9.5−10.5 (Figure 4B,C) and 1000−5000 ms in pH 11−12 (Figure 4D). The initial flat portion of the kinetic trace (readily discernible in Figure 4A) represents a dead time of 1.5−2 ms of the stopped-flow and was excluded for model analysis of reaction rate constant. Since the first-order rate constant is independent of the initial concentration of reactants, exclusion of this portion does not affect the rate calculation. The kinetic spectral scans over the wavelength range of 225−315 nm at various pH values are shown in Figure 5. It is clear that MCA is produced at 243 nm with OCl^- being consumed at 294 nm. The time interval is equal between two neighboring curves.

The pseudo-first-order rate constant (k_{obs}') is readily obtained by model fitting the kinetic traces in Figure 4, and the second-order rate constant (k_{obs}'') is then calculated by dividing k_{obs}' by the initial concentration of ammonia. Our

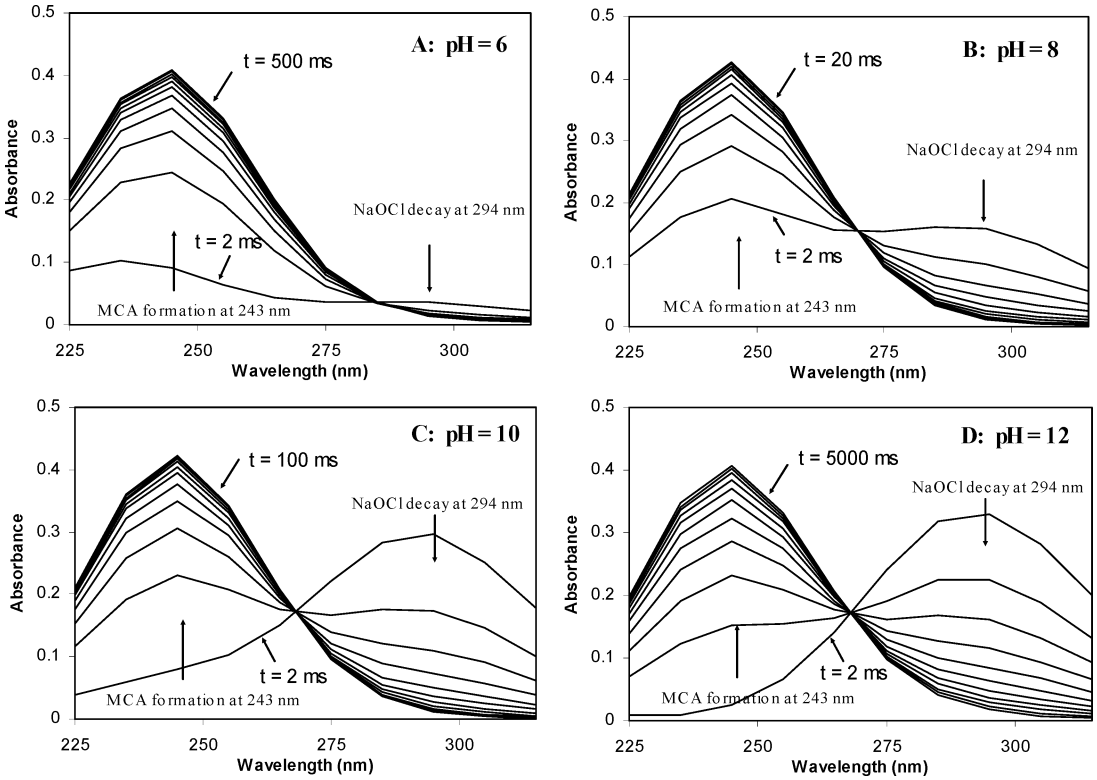

FIGURE 5. Kinetic spectral scans of MCA formation reaction: (A) pH 6; (B) pH 8; (C) pH 10; (D) pH 12. Experimental conditions: same as in Figure 4.

TABLE 1. Measured Pseudo-First-Order Rate Constants and Derived Second-Order Rate Constants of MCA Formation as a Function of pH

$[NH_4Cl]$ (mM)	[HOCl] (mM)	pH_o	pH_f	pH_{av}	k_{obs}' (s^{-1}) OCl^-	k_{obs}' (s^{-1}) MCA	k_{obs}'' ($M^{-1}\cdot s^{-1}$) MCA	time (ms)
10	1	6.00	5.48	5.74	19.22 ± 0.42	14.76 ± 0.04	1476	500
10	1	6.50	6.34	6.42	42.46 ± 0.18	36.08 ± 0.22	3608	200
10	1	7.00	6.90	6.95	103.38 ± 0.41	88.76 ± 0.37	8876	50
10	1	7.50	7.39	7.45	192.4 ± 0.79	180.0 ± 0.78	18000	20
10	1	7.80	7.72	7.76	245.42 ± 0.84	244.94 ± 0.84	24494	20
10	1	8.00	7.92	7.96	264.02 ± 0.88	260.7 ± 1.37	26070	20
10	1	8.50	8.50	8.50	283.64 ± 1.26	294.42 ± 2.59	29442	20
10	1	9.00	9.02	9.01	234.86 ± 1.14	246 ± 0.92	24600	20
10	1	9.50	9.59	9.55	134.94 ± 0.91	143.62 ± 0.59	14362	50
10	1	9.80	9.93	9.87	83.92 ± 0.33	85.42 ± 0.23	8542	50
10	1	10.00	10.04	10.02	63.74 ± 0.4	64.16 ± 0.39	6416	100
10	1	10.50	10.60	10.55	23.36 ± 0.12	23.76 ± 0.04	2376	200
10	1	11.00	11.12	11.06	7.64 ± 0.06	7.66 ± 0.01	766	1000
10	1	11.50	11.50	11.50	2.37 ± 0.013	2.38 ± 0.005	238	2000
10	1	12.00	12.00	12.00	0.72 ± 0.002	0.72 ± 0.002	72	5000

data analysis indicates that all kinetic traces are well fitted by the pseudo-first-order equation. The values of k_{obs}' and k_{obs}'' from pH 6 to 12 are compiled in Table 1. The plot of k_{obs}'' against reaction pH (the average of the original and final pH values) indicates that the k_{obs}'' first increases with increasing pH up to pH 8.5 and then decreases as the pH further increases (Figure 6).

The maximum k_{obs}'' appears at pH 8.5 which approximates the arithmetic mean of $pK_{a,Cl}$ and $pK_{a,N}$ (pH 8.39, theoretically). This pH is similar to those observed by others, i.e., pH 8.2 (*6*) and pH 8.0 (*8*).

The pH associated with the peak rate can be theoretically deduced. Taking reaction 9 as an example, the rate of MCA formation reaches the maximum at the pH where the product of [HOCl]·[NH_3] reaches the maximum (see eq 13). This pH can be determined by taking the derivative of [HOCl]·[NH_3] over {H^+}:

$$\frac{d([HOCl][NH_3])}{d\{H^+\}} = \frac{d}{d\{H^+\}}\left(\frac{[HOCl]_T[NH_3]_T}{\left(1+\frac{K_{a,Cl}}{\gamma\{H^+\}}\right)\left(1+\frac{\{H^+\}}{\gamma K_{a,N}}\right)}\right) = \frac{[HOCl]_T[NH_3]_T K_{a,N}\gamma^3}{(K_{a,Cl}+\gamma\{H^+\})^2(\gamma K_{a,N}+\{H^+\})^2}\cdot[K_{a,Cl}K_{a,N}-\{H^+\}^2] \quad (24)$$

Mathematically, the product of [HOCl]·[NH_3] reaches the maximum when the derivative equals zero. Thus

$$\{H^+\}^2 = K_{a,Cl}K_{a,N} \quad (25)$$

Taking the −log of both sides gives

$$pH = \frac{1}{2}(pK_{a,Cl} + pK_{a,N}) \quad (26)$$

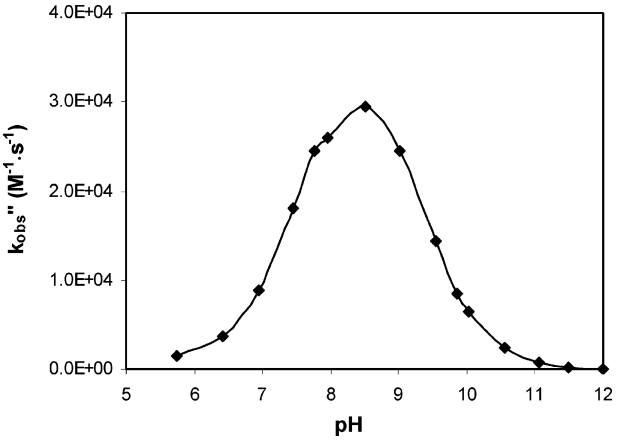

FIGURE 6. Plot of the observed second-order rate constant against average pH.

TABLE 2. Effect of NH_4Cl and HOCl Concentrations on the MCA Formation Rate

$[NH_4Cl]$ (mM)	[HOCl] (mM)	k_{obs}' (s^{-1})	k_{obs}'' ($M^{-1}\cdot s^{-1}$)	time (ms)
20	2	577.2 ± 3.45	28860	20
30	2	857.12 ± 10.54	28571	10
40	2	1109.8 ± 4.48	27745	10
10	1	286.74 ± 1.29	28674	20
15	1	428.94 ± 3.45	28596	20
20	1	569.8 ± 2.61	28490	20
5	0.5	145.52 ± 1.20	29104	50
7.5	0.5	213.86 ± 1.52	28515	50
10	0.5	288.74 ± 1.66	28874	50

Similarly, we have the following equations for reactions 10−12, respectively:

$$\frac{d([HOCl][NH_4^+])}{d\{H^+\}} = \frac{[HOCl]_T[NH_3]_T\gamma\{H^+\}^2}{(K_{a,Cl}+\gamma\{H^+\})^2(\gamma K_{a,N}+\{H^+\})^2}\cdot \left[\gamma^2 K_{a,N} + \frac{2\gamma K_{a,Cl}K_{a,N}}{\{H^+\}} + K_{a,Cl}\right] \quad (27)$$

$$\frac{d([OCl^-][NH_3])}{d\{H^+\}} = \frac{[HOCl]_T[NH_3]_T K_{a,Cl}K_{a,N}\gamma}{(K_{a,Cl}+\gamma\{H^+\})^2(\gamma K_{a,N}+\{H^+\})^2}\cdot [-(\gamma^2 K_{a,N} + 2\gamma\{H^+\} + K_{a,Cl})] \quad (28)$$

$$\frac{d([OCl^-][NH_4^+])}{d\{H^+\}} = \frac{[HOCl]_T[NH_3]_T K_{a,Cl}\gamma}{(K_{a,Cl}+\gamma\{H^+\})^2(\gamma K_{a,N}+\{H^+\})^2}\cdot [K_{a,Cl}K_{a,N} - \{H^+\}^2] \quad (29)$$

Equation 27 implies a value always greater than zero, and eq 28 implies a value always less than zero because each term in the right-hand side of both equations has a positive value. If reactions 10 and 11 dominated, there would be no peak rate appearing in Figure 6. Therefore, these two reactions are insignificant. Equation 29 yields the same result as eq 24 since the nonionic and ionic reactions are symmetric in formula. If reaction 12 dominates, a peak rate is also observable at the pH determined by eq 26. It is not possible to tell which reaction is predominant only from the kinetic viewpoint because reactions 9 and 12 have the same pH dependence.

It is noted that there is a discrepancy between the pseudo-first-order rate constants of OCl^- decay and MCA production below pH 10 because the protonation of OCl^- or deprotonation of HOCl interfered with the measurement of OCl^- absorbance. In this study, the rate of MCA production was used for model computations.

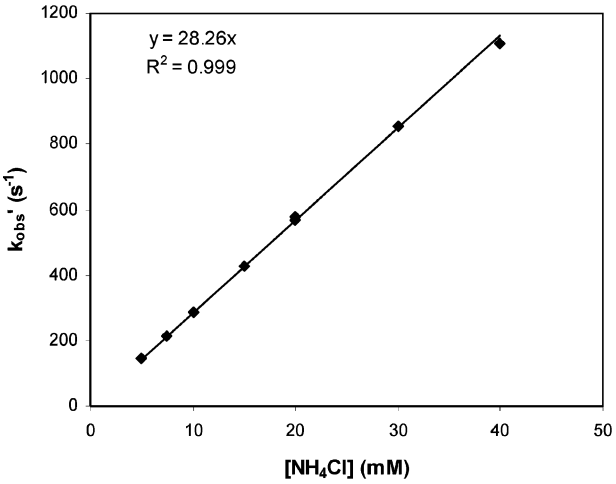

FIGURE 7. Measured pseudo-first-order rate constant as a function of NH_4Cl concentration. Experimental conditions: pH 8.5, 50 mM $NaClO_4$, 10 mM phosphate buffer, 25 °C.

TABLE 3. Temperature Dependence of the Ionization Constants of Hypochlorous Acid and Ammonia

T (°C)	$pK_{a,Cl}$[a] HOCl/OCl^-	$pK_{a,N}$[b] NH_4^+/NH_3
5	7.754	9.903
15	7.633	9.567
25	7.537	9.251
35	7.463	8.955

[a] Ref *14*. [b] Calculated from ref *15*.

TABLE 4. Derived Second-Order Rate Constants of MCA Formation as a Function of pH and Temperature

	T = 5 °C		T = 15 °C		T = 35 °C	
pH_o	pH_{av}	k_{obs}'' ($M^{-1}\cdot s^{-1}$)	pH_{av}	k_{obs}'' ($M^{-1}\cdot s^{-1}$)	pH_{av}	k_{obs}'' ($M^{-1}\cdot s^{-1}$)
6.00	5.79	332	5.77	1396	5.73	3822
7.00	6.94	1857	6.94	4062	6.94	18010
7.50	7.43	4209	7.44	8919	7.44	36600
8.00	7.97	6489	7.95	13046	7.94	48100
9.00	9.11	6012	9.06	12544	8.96	44980
9.50	9.60	3722	9.57	7595	9.48	28178
10.00	10.04	2602	10.02	4394	10.02	8939
11.00	11.09	241	11.07	498	11.03	1384
12.00	12.03	18.4	12.02	40.0	11.96	156

Effect of NH_4Cl and HOCl Concentrations. At pH 8.5, the effect of ammonia and free chlorine concentrations on the rate of MCA formation was investigated. The HOCl concentration varied from 0.5 to 2 mM, while the NH_4Cl concentration was prepared in accordance with the molar ratios ($[NH_4Cl]/[HOCl]$) of 10:1, 15:1, and 20:1.

The measured pseudo-first-order and derived second-order rate constants are compiled in Table 2. The plot of k_{obs}' against NH_4Cl concentration indicates that the reaction rate is independent of the initial HOCl concentration but linearly proportional to the NH_4Cl concentration (Figure 7). This behavior can be explained by eqs 5 and 6. The k_{obs}' does not rely on the initial concentration of HOCl as the pseudo-first-order kinetic equation (eq 5) is applicable. On the other hand, k_{obs}' is equal to the product of total NH_3 concentration and k_{obs}'', as shown in eq 6. The k_{obs}' thus increases linearly with increasing NH_4Cl concentration. The slope in Figure 7

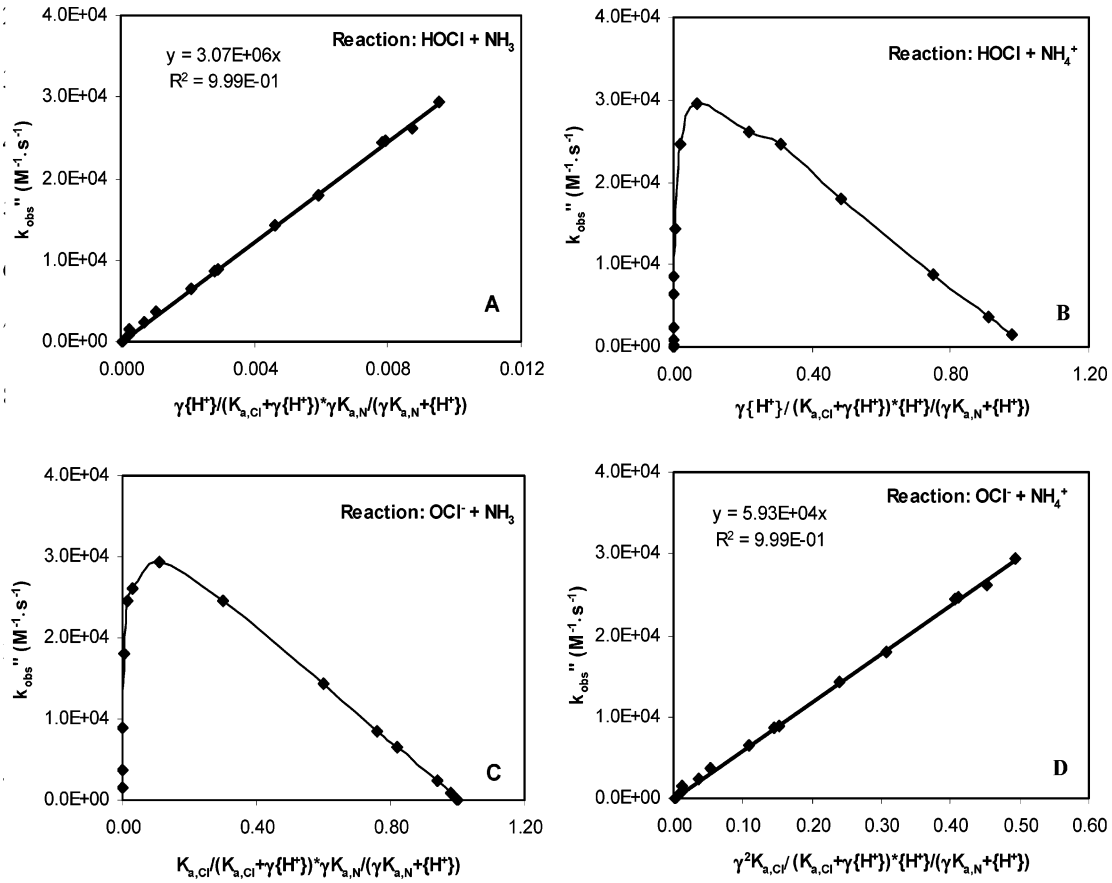

FIGURE 8. Plot of the observed second-order rate constants against the activity product of reacting species: (A) HOCl + NH_3; (B) HOCl + NH_4^+; (C) OCl^- + NH_3; (D) OCl^- + NH_4^+. Experimental conditions: same as in Figure 4.

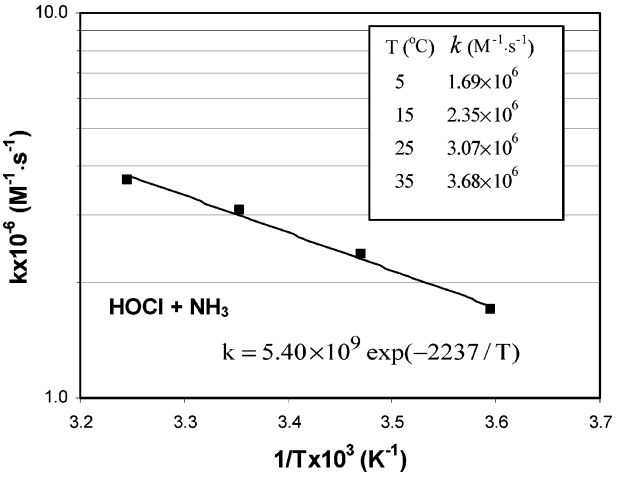

FIGURE 9. Arrhenius plot for the nonionic pathway.

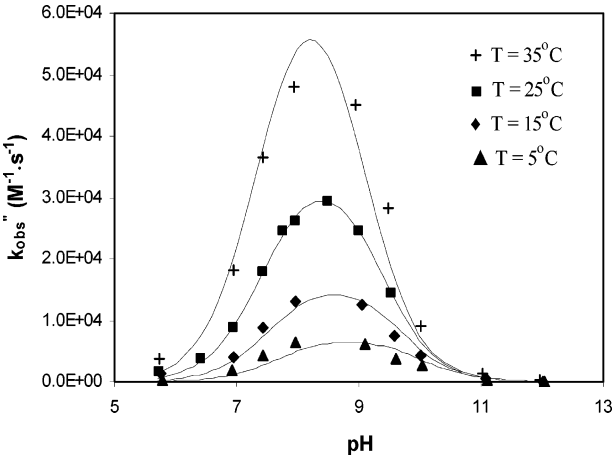

FIGURE 10. Model fit of the experimental second-order rate constants at various temperatures and pH values: symbols-experimental data points, solid lines-model fitting curve.

(28260 $M^{-1}\cdot s^{-1}$) is equal to k_{obs}''. This demonstrates that the pseudo-first-order approximation is sound at $[NH_4Cl]_T/[HOCl]_T \geq 10{:}1$.

Determination of Specific Rate Constants. As mentioned in the model description, the analysis of specific rate constants is based on the speciation of reactants. The derived second-order rate constant (k_{obs}'') and average pH in Table 1 are used to model the specific rate constants using eqs 18−21. The plot of k_{obs}'' against the activity product of reacting species in Figure 8B,C clearly indicates that neither reaction 10 (HOCl + NH_4^+) nor reaction 11 (OCl^- + NH_3) is possible. In other words, if these two reactions occurred, the plot of k_{obs}'' vs their activity product would have yielded a straight line as described by eqs 19 and 20. These results agree with the conclusion drawn from the pH dependence of the MCA formation rate previously mentioned. Results also show that either reaction 9 (HOCl + NH_3) or reaction 12 (OCl^- + NH_4^+) is the potential pathway for MCA formation, with k_{HOCl,NH_3} equaling 3.07×10^6 $M^{-1}\cdot s^{-1}$ ($R^2 = 0.999$) or k_{OCl^-,NH_4^+} equaling 5.93×10^4 $M^{-1}\cdot s^{-1}$ ($R^2 = 0.999$). The value of k_{HOCl,NH_3} agrees well with that reported by Johnson and Inman (*10*), i.e., 3.1×10^6 $M^{-1}\cdot s^{-1}$ at 25 °C. These researchers determined the rate of MCA formation in artificial seawater with salinities ranging from 0.1 to 2%, but the effect of ionic strength was carefully corrected. Weil and Morris (*6*) reported a value of 6.2×10^6 $M^{-1}\cdot s^{-1}$ but seemed to be limited by both instrumentation and experimental design. In a later critical

review paper, Morris and Isaac (*12*) approximated a specific rate constant of 4.2×10^6 $M^{-1}\cdot s^{-1}$ using the quite scattered data collected from the literature (*6*, *10*−*11*). The rate constants reported by Morris and coauthors (*6*, *12*) have been extensively cited by journal papers and environmental books (*1*, *2*, *7*), while Johnson and Inman's rate constant has little citation. This is most likely due to their work being conducted in artificial seawater (*10*), and other researchers probably oversaw their correction for ionic strength. Recently, Suddiqui (*22*) reported a rate constant of 100 $M^{-1}\cdot s^{-1}$ though this value is suspect because no experimental evidence was provided.

Though k_{OCl^-,NH_4^+} is only about 2% of k_{HOCl,NH_3}, our kinetic results show that this ionic pathway is still plausible from strictly kinetic considerations because the activity product of the two ionic species can be higher than that of two nonionic species. It seems impossible to determine which pathway really contributes to MCA formation only from the kinetic point of view. The same question was raised by Wei and Morris (*6*). Mechanistically, however, the ionic pathway is implausible. Hoigné et al. (*23*) reported that ozone reacts with NH_3 at a second-order rate constant of 20 ± 2 $M^{-1}\cdot s^{-1}$, but ozone is totally nonreactive toward NH_4^+. If the electrophilic attack of ozone on NH_4^+-N does not occur, analogously the electrophilic attack of OCl^--Cl on NH_4^+-N will also be unlikely. Most researchers have agreed that MCA is only generated by the elementary reaction between the neutral molecules of HOCl and NH_3 (*10*, *12*).

In brief, the two hybrid reactions between one neutral molecule and one ionic species can be kinetically excluded as the potential pathways for MCA generation. The ionic reaction is implausible from the mechanistic point of view. Thus, the only reaction accounting for MCA generation is the nonionic pathway. At this point, we are now able to substantiate our previous assumption that only one reaction dominates the generation of MCA in the model description section.

Effect of Ionic Strength and Buffer Concentrations. This set of experiments applied 5 mM KH_2PO_4 as buffer and 10 mM $NaClO_4$ as ionic strength control. The initial concentrations of NH_4Cl and HOCl were prepared at 20 and 2 mM, respectively. The reaction pH ranged from 6.5 to 11.5. Under these conditions, the total ionic strength was approximately equal to 0.037 M, and the activity coefficient (γ) was calculated to be 0.83. Results show that k_{HOCl,NH_3} is equal to 3.07×10^6 $M^{-1}\cdot s^{-1}$ ($R^2 = 0.992$), which is identical to that determined previously under the experimental conditions of 10 mM buffer and 50 mM ionic strength control. It is seen that the ionic strength and buffer concentrations have no notable effect on the determination of specific rate constants as long as the activity coefficients are incorporated into model computations.

Arrhenius Plot. The rate of a chemical reaction is usually a function of temperature which can be expressed by the Arrhenius equation

$$k = A\cdot e^{-E_a/RT} \tag{30}$$

where k = rate constant, A = frequency factor, E_a = activation energy, R = universal gas constant (8.315 $J\cdot K^{-1}\cdot mol^{-1}$), and T = absolute temperature (K). After transformation, this equation becomes

$$\ln(k) = \ln(A) - E_a/RT \tag{31}$$

Thus, the plot of ln(k) vs $1/T$ will yield a linear curve with an intercept equaling ln(A) and a slope equaling $-E_a/R$.

The effect of temperature on the rate of MCA formation was investigated from 5 to 35 °C. This range represents the typical temperature condition in drinking water and wastewater treatment systems. It should be pointed out that the ionization constant is also a function of temperature. Morris (*14*) determined the ionization constant of aqueous HOCl from 5 to 35 °C. Thurston et al. (*15*) tabulated the percent of un-ionized ammonia for aqueous ammonia equilibrium from 0 to 40 °C. Bates and Pinching (*24*) also reported a temperature function of the ionization constant of ammonia. It is found that the *pK* values of ammonia are in good agreement in the two sources (*15*, *24*), i.e., less than 0.02 pH units. Therefore, it is expected that the *pK* values of HOCl and NH_3 have no high variability in published data. The data from Morris (*14*) and Thurston (*15*) are compiled in Table 3, which were used for model analysis of the specific rate constants of MCA formation at given temperatures. It is seen that as the temperature changes from 5 to 35 °C, $pK_{a,Cl}$ and $pK_{a,N}$ change by 0.29 and 0.94 pH units, respectively. This significant change makes it important to correct the ionization constants by temperature.

The derived second-order rate constants (k_{obs}'') at various temperatures and pH values are shown in Table 4. Results indicate that the k_{obs}'' increases rapidly with increasing temperature at a given pH. Plotting k_{obs}'' vs the activity product using eq 18 yields k_{HOCl,NH_3}. The values of k_{HOCl,NH_3} at various temperatures are shown in the insert of Figure 9. From these data, the Arrhenius equation for the nonionic pathway is obtained as follows (Figure 9):

$$k_{HOCl,NH_3} = 5.40 \times 10^9 \exp(-2237/T) \tag{32}$$

The activation energy is calculated to be 18.6 $kJ\cdot mol^{-1}$. The Arrhenius equation and activation energy achieved in this work are considerably different from those approximated by Morris and Isaac (*12*), i.e., $k = 6.6 \times 10^8 \exp(-1510/T)$ and 12.6 $kJ\cdot mol^{-1}$.

With the specific rate constants (k_{HOCl,NH_3}) at various temperatures available, the second-order rate constant (k_{obs}'') at any pH can be readily calculated by the proposed model (eq 18). Results in Figure 10 demonstrate a good fit between the experimentally determined rate constants and the model fitting curve.

Acknowledgments

The authors gratefully acknowledge the financial support from U.S. EPA for this research project under the contract number of XP-99795901-0 and the support and guidance from the project officer, Dr. R. Y. Surampalli. The authors also wish to thank the graduate student Evelyn Chamberlain for her assistance on experimental work.

Literature Cited

(1) Snoeyink, V. L.; Jenkins, D. *Water Chemistry*; John Wiley: New York, 1980; p 396.
(2) Jafvert, C. T.; Valentine, R. L. *Environ. Sci. Technol.* **1992**, *26*, 577−586.
(3) White, G. C. *Handbook of Chlorination and Alternative Disinfectants, Volume 3;* Van Nostrand Reinhold Co.: New York, 1992.
(4) *Alternative Disinfectants and Oxidants Guidance Manual*; U.S. EPA 815-R-99-014; U.S. Environmental Protection Agency, Office of Water: Washington, DC, April 1999.
(5) Ward, N. R.; Wolfe, R. L.; Olson B. H. *Appl. Environ. Microbiol.* **1984**, *48*, 508−514.
(6) Weil, I.; Morris J. C. *J. Am. Chem. Soc.* **1949**, *71*, 1664−1671.
(7) Anbar, M.; Yagil, G. *J. Am. Chem. Soc.* **1962**, *84*, 1790−1796.
(8) Patton, C. J.; Crouch, S. R. *Anal. Chem.* **1977**, *49*, 464−469.
(9) Margerum, D. W.; Gray, E. T., Jr.; Huffman, R. P. In *Organometals and Organometalloids; Occurrence and Fate in the Environment*; ACS Symposium Series 82; Brinckman, F. E., Bellama, J. M., Ed.; American Chemical Society: Washington, DC, 1978; pp 278−291.
(10) Johnson, J. D.; Inman, G. W., Jr. *The Kinetics of Chlorine-Ammonia Reactions in Seawater*; NUREG/CR-0528; NTIS: Springfield, VA, 1978.

(11) Isaac, R. A. Ph.D. Thesis, Harvard University, Cambridge, MA, 1981.
(12) Morris, J. C.; Isaac R. A. In *Water Chlorination, Environmental Impact and Health Effects*; Jolley, R. L., et al., Ed.; Ann Arbor Science: Ann Arbor, MI, 1983; Vol. 4, Chapter 2.
(13) Evans, O. M. *Anal. Chem.* **1982**, *54*, 1579−1582.
(14) Morris, J. C. *J. Phys. Chem.* **1966**, *70*, 3798−3805.
(15) Thurston, R. V.; Russo, R. C.; Emerson, K. *Aqueous Ammonia Equilibrium-Tabulation of Percent Un-ionized Ammonia*; U.S. EPA-600/3-79-091; NTIS: Springfield, VA, 1979.
(16) Stumm, W.; Morgan, J. J. *Aquatic Chemistry: An Introduction Emphasizing Chemical Equilibria in Natural Waters*, 2nd ed.; John Wiley: New York, 1981; pp 99−103, 135, 414.
(17) Gray, E. T., Jr. Ph.D. Thesis, Purdue University, West Lafayette, IN, 1977.
(18) Gray, E. T., Jr.; Margerum, D. W.; Huffman, R. P. In *Organometals and Organometalloids; Occurrence and Fate in the Environment*; ACS Symposium Series 82; Brinckman, F. E., Bellama, J. M., Eds.; American Chemical Society: Washington, DC, 1978; pp 264−277.
(19) Isaac, R. A.; Morris, J. C. *Environ. Sci. Technol.* **1983**, *17*, 738−742.
(20) Hand, V. C.; Margerum, D. W. *Inorg. Chem.* **1983**, *22*, 1449−1456.
(21) Jafvert, C. T.; Valentine, R. L. *Water Res.* **1987**, *21*, 967−973.
(22) Siddiqui, M. S. *Water Res.* **1996**, *30*, 2160−2170.
(23) Hoigné, J.; Bader, H.; Haag, W. R.; Staehelin, J. *Water Res.* **1985**, *19*, 993−1004.
(24) Bates, R. G.; Pinching, G. D. *J. Am. Chem. Soc.* **1950**, *72*, 1393−1396.

Received for review July 11, 2003. Revised manuscript received November 25, 2003. Accepted December 14, 2003.

ES0347484